

# Engineered Swift Equilibration for Arbitrary Geometries

Adam G. Frim,<sup>1,\*</sup> Adrienne Zhong,<sup>1</sup> Shi-Fan Chen,<sup>1</sup> Dibyendu Mandal,<sup>1</sup> and Michael R. DeWeese<sup>1,2,†</sup>

<sup>1</sup>*Department of Physics, University of California, Berkeley, Berkeley, CA, 94720*

<sup>2</sup>*Redwood Center For Theoretical Neuroscience and Helen Wills Neuroscience Institute, University of California, Berkeley, Berkeley, CA, 94720*

(Dated: May 15, 2022)

Engineered swift equilibration (ESE) is a class of driving protocols that enforce an instantaneous equilibrium distribution with respect to external control parameters at all times during rapid state transformation of open, classical non-equilibrium systems. ESE protocols have previously been derived and experimentally realized for Brownian particles in simple, one-dimensional, time-varying trapping potentials; one recent study considered ESE in two-dimensional Euclidean configuration space. Here we extend the ESE framework to generic, overdamped Brownian systems in arbitrary curved configuration spaces and illustrate our results with specific examples not amenable to previous techniques. Our approach may be used to impose the necessary dynamics to control the full configurational distribution in a wide variety of experimentally realizable settings.

*Introduction.*—In any process that transforms a system from one state to another, there exists some intrinsic relaxation time for the final state to be reached. Recently, a number of studies have attempted to manipulate or, in principle, eliminate altogether this relaxation time by means of alternative driving protocols. Such strategies are generally known as shortcuts to adiabaticity (STA), in which one attempts to rapidly transform from a specified initial state or distribution at time  $t_0$  to a target state at a specified final time  $t_f$  [1–7]. These types of protocols have seen success in a variety of settings, including both open and closed quantum and classical systems. A more specific class of strategies goes by the name of Engineered Swift Equilibration (ESE) and focuses on enforcing internal equilibrium in an open classical system during the entire transformation [8–11]. This is typically done by means of an added driving force: in essence, by following a specified driving protocol, a rapidly-transforming system assumes the trajectory of a quasistatic transformation.

To make this more concrete, consider a physical system described by some time-dependent Hamiltonian  $H(\lambda_i(t))$ , where  $t$  is the time, and all time dependence is prescribed by parameters  $\lambda_i(t)$ . Following standard Boltzmann statistics [12], the equilibrium probability distribution at a given time is

$$\rho_{\text{eq}}(\mathbf{x}; \lambda_i(t)) = \frac{\exp(-\beta H_0(\mathbf{x}; \lambda_i(t)))}{Z(\lambda_i(t))}, \quad (1)$$

where  $\beta = (k_B T)^{-1}$  is the inverse temperature,  $k_B$  is Boltzmann’s constant, and  $Z(\lambda_i(t))$  is the partition function, explicitly dependent on parameters  $\lambda_i(t)$ . If the  $\{\lambda_i(t)\}$  are changed adiabatically, the system will be well-described by Boltzmann statistics at all times. However, if  $\lambda_i(t)$  changes sufficiently rapidly, the system deviates from its equilibrium distribution specified by Eq. (1). The purpose of ESE is to introduce a modified Hamiltonian  $H(\mathbf{x}, t) = H_0(\mathbf{x}, \lambda_i(t)) + H_1(\mathbf{x}, t)$  such that under the full dynamics of  $H$ , the system assumes the inter-

nal equilibrium distribution of  $H_0$  alone [Eq. (1)], at all times.

To date, ESE protocols have been successfully derived for a Brownian particle trapped in a variety of simple one-dimensional potentials [13, 14] and realized experimentally for a Brownian particle in a 1D harmonic trap [8]. The framework was also recently analytically solved for the Brownian gyrator [15], a two-dimensional (Euclidean) system in contact with two heat baths that admits non-equilibrium steady states. In this letter, we extend the ESE framework to generic overdamped Brownian systems, including those with arbitrarily high dimensional, non-Euclidean configuration spaces. We demonstrate the utility of our framework by numerically finding the ESE forcing for previously intractable systems.

*Theory.*—We first consider a particle undergoing Brownian motion in the overdamped limit, whose dynamics are governed by the Langevin equation:

$$\gamma \frac{d\mathbf{x}(t)}{dt} = -\nabla V(\mathbf{x}(t); \lambda_i(t)) + \boldsymbol{\eta}(t) + \mathbf{F}_{\text{ext}}(t), \quad (2)$$

where  $\mathbf{x}$  is the position of the particle,  $\gamma$  is the viscosity,  $V(\mathbf{x}; \lambda_i(t))$  is the potential acting on the particle parameterized by control parameters  $\lambda_i(t)$ ,  $\boldsymbol{\eta}$  is Gaussian noise with delta function autocorrelation  $\langle \eta_i(t) \eta_j(t') \rangle = (2\gamma/\beta) \delta_{ij} \delta(t - t')$ , where  $i, j$  index Euclidean coordinates and  $\mathbf{F}_{\text{ext}}(t)$  is an external force on the particle.

Following standard procedures [12], this leads to a Fokker-Planck equation of the form:

$$\partial_t \rho(\mathbf{x}, t) = \nabla \cdot \left[ \left( \frac{\nabla V(\mathbf{x}; \lambda_i(t)) - \mathbf{F}_{\text{ext}}}{\gamma} + \frac{\nabla}{\beta\gamma} \right) \rho(\mathbf{x}, t) \right], \quad (3)$$

where  $\rho(\mathbf{x}, t)$  is the configuration space probability distribution at a given time. In the absence of an external force, the steady state solution is found by taking the LHS of Eq. (3) to zero, yielding the usual Boltzmann distribution,  $\rho_{\text{eq}}$ .

Now suppose that the control parameters  $\lambda_i(t)$  are time-dependent, and varied quickly enough so that we cannot assume a quasistatic transition. We desire to find a  $\mathbf{F}_{\text{ext}}(t)$  such that  $\rho(\mathbf{x}(t), t; \lambda_i(t)) = \rho_{\text{eq}}(\mathbf{x}; \lambda_i(t))$  for all times  $t$ . Clearly, this can only be satisfied if all explicitly time-dependent terms in Eq. (3) independently cancel. Defining  $\mathbf{P} \equiv \rho_{\text{eq}} \mathbf{F}_{\text{ext}}$ , this constrain can be written

$$\nabla \cdot \mathbf{P} = -\gamma \partial_t \rho_{\text{eq}}. \quad (4)$$

We now generalize to systems whose configuration space is an arbitrary compact, orientable Riemannian manifold  $M$  with metric  $g$ , and write the vector  $\mathbf{P}$  as a differential one-form  $P = P_i dx^i$ . Equation (4) then generalizes to

$$d^\dagger P = -\gamma \partial_t \rho_{\text{eq}}, \quad (5)$$

where  $d$  is the exterior derivative and  $d^\dagger$  is its Hodge dual:  $d^\dagger = \star d \star$ , where  $\star$  is the Hodge star operator. We now invoke the Hodge Decomposition, which states that, for any  $k$ -form  $P_k$  on  $M$ , there exists a unique decomposition [16]:

$$P_k = dA_{k-1} + d^\dagger B_{k+1} + C_k, \quad (6)$$

where  $A_{k-1}$  and  $B_{k+1}$  are  $(k-1)$ - and  $(k+1)$ -forms, respectively, and  $C_k$  is a harmonic  $k$ -form; *i.e.*  $\Delta C_k = 0$ , and  $\Delta = dd^\dagger + d^\dagger d$  is the generalized Laplace operator. Therefore, we may write Eq. (4) as

$$d^\dagger P = d^\dagger(dA + d^\dagger B + C) = d^\dagger dA + d^\dagger C = \Delta A + d^\dagger C, \quad (7)$$

where  $A$  is a 0-form,  $B$  is a 2-form, and  $C$  is a harmonic 1-form. For simplicity, we choose  $C = 0$  to yield a generalized Poisson's equation:

$$\Delta A = -\gamma \partial_t \rho_{\text{eq}}. \quad (8)$$

Using this result, coupled with Eq. (6), we arrive at our main result:

$$\mathbf{F}_{\text{ext}} = \frac{dA}{\rho_{\text{eq}}}. \quad (9)$$

To demonstrate the utility of this expression, we now apply it to multiple physically realizable example systems.

*Higher Dimensional Euclidean Configuraton Space.*— In a  $d$ -dimensional Euclidean space, the Hodge decomposition trivializes to the Helmholtz decomposition [16]. Our results still hold, though for certain cases the decomposition may no longer be unique. Noting this caveat, we continue with our analysis. For this space, the generalized Laplace operator is simply the standard Laplace operator. Note that our choice  $C = 0$  amounts to a no-curl gauge:  $\nabla \times \mathbf{P} = 0$ . We may thus define a scalar potential  $A$  that satisfies  $\nabla A = \mathbf{P}$ . This is analogous to standard electrostatics, where  $A$  and  $\mathbf{P}$  play of the roles the electric potential and field, respectively [17].

Given the general solution to the Laplace operator for Euclidean space, we have, for  $d \neq 2$ ,

$$A(\mathbf{x}) = -\frac{\Gamma(\frac{d-2}{2})}{4\pi^{\frac{d}{2}}} \int d^d \mathbf{x}' |\mathbf{x} - \mathbf{x}'|^{2-d} (-\gamma \partial_t \rho_{\text{eq}}(\mathbf{x}')) \quad (10)$$

and  $\mathbf{F}_{\text{ext}}(\mathbf{x}) = \rho_{\text{eq}}^{-1} \nabla A$ . Note that this solution reproduces Eq. (12) of [13] for 1D systems. For the special case of  $d = 2$ , the potential is given by

$$A(\mathbf{x}) = \frac{1}{2\pi} \int d^2 \mathbf{x}' \log |\mathbf{x} - \mathbf{x}'| (-\gamma \partial_t \rho_{\text{eq}}(\mathbf{x}')). \quad (11)$$

*Spherical Configuration Space.*— We now consider topologically nontrivial configuration spaces. As a first example, consider an electric dipole with dipole moment  $\mathbf{p} = p \hat{\mathbf{p}}$  placed in a time-varying electric field pointed in the  $z$ -direction,  $\mathbf{E} = E(t) \hat{\mathbf{z}}$ , as shown in Fig. 1(a). The potential energy for this system is

$$V(\theta, \phi, t) = -pE(t) \cos(\theta), \quad (12)$$

where  $\cos \theta = \hat{\mathbf{p}} \cdot \hat{\mathbf{z}}$  and  $\phi$  measures the azimuthal angle about to the  $z$ -axis. The configuration space of this system is the 2-sphere,  $M = S^2$ , for which the Laplace operator is

$$\Delta_{S^2} = \frac{1}{\sin \theta} \frac{\partial}{\partial \theta} \left( \sin \theta \frac{\partial}{\partial \theta} \right) + \frac{\partial^2}{\partial \phi^2}. \quad (13)$$

To calculate the required ESE force, we find  $\rho_{\text{eq}}(t)$ , the instantaneous Boltzmann distribution for this system:

$$\rho_{\text{eq}}(t) = \left[ \frac{4\pi \sinh(\beta p E(t))}{\beta p E(t)} \right]^{-1} \exp \beta p E(t) \cos \theta, \quad (14)$$

such that the governing equation is given by  $\Delta_{S^2} A = -\gamma \partial_t \rho_{\text{eq}}$ . In the high temperature limit, one may find an analytic expression for  $A$  (see Supplemental Materials Section SM.1 for details ); however, finding a closed-form expression is, in general, intractable. Instead, we employ a series expansion in the spherical harmonics,  $Y_\ell^m(\theta, \phi)$ . The spherical harmonics are the eigenfunctions of the spherical Laplace operator, *i.e.*  $\Delta_{S^2} Y_\ell^m(\theta, \phi) = -\ell(\ell+1) Y_\ell^m(\theta, \phi)$ , such that if we write  $\rho_{\text{eq}} = \sum_{\ell, m} c_{\ell, m}(t) Y_\ell^m(\theta, \phi)$ , then by the orthogonality and completeness of the spherical harmonics, we have

$$A = \gamma \sum_{\ell=0}^{\infty} \sum_{m=-\ell}^{\ell} \frac{\partial_t c_{\ell, m}(t)}{\ell(\ell+1)} Y_\ell^m(\theta, \phi). \quad (15)$$

Note that  $c_{\ell, m}$  may likewise be computed:

$$c_{\ell, m}(t) = \int_{\Omega} \rho_{\text{eq}}(\theta, \phi, t) Y_\ell^{m*}(\theta, \phi) d\Omega. \quad (16)$$

Due to the azimuthal symmetry of  $\rho_{\text{eq}}(\theta, \phi, t)$ , only  $m = 0$  terms will be nonzero, simplifying our analysis. Finally,  $\mathbf{F}_{\text{ext}}$  is found by taking  $\mathbf{P} = dA \implies \mathbf{F}_{\text{ext}} = \rho_{\text{eq}}^{-1} (\nabla_{S^2}) A$ .

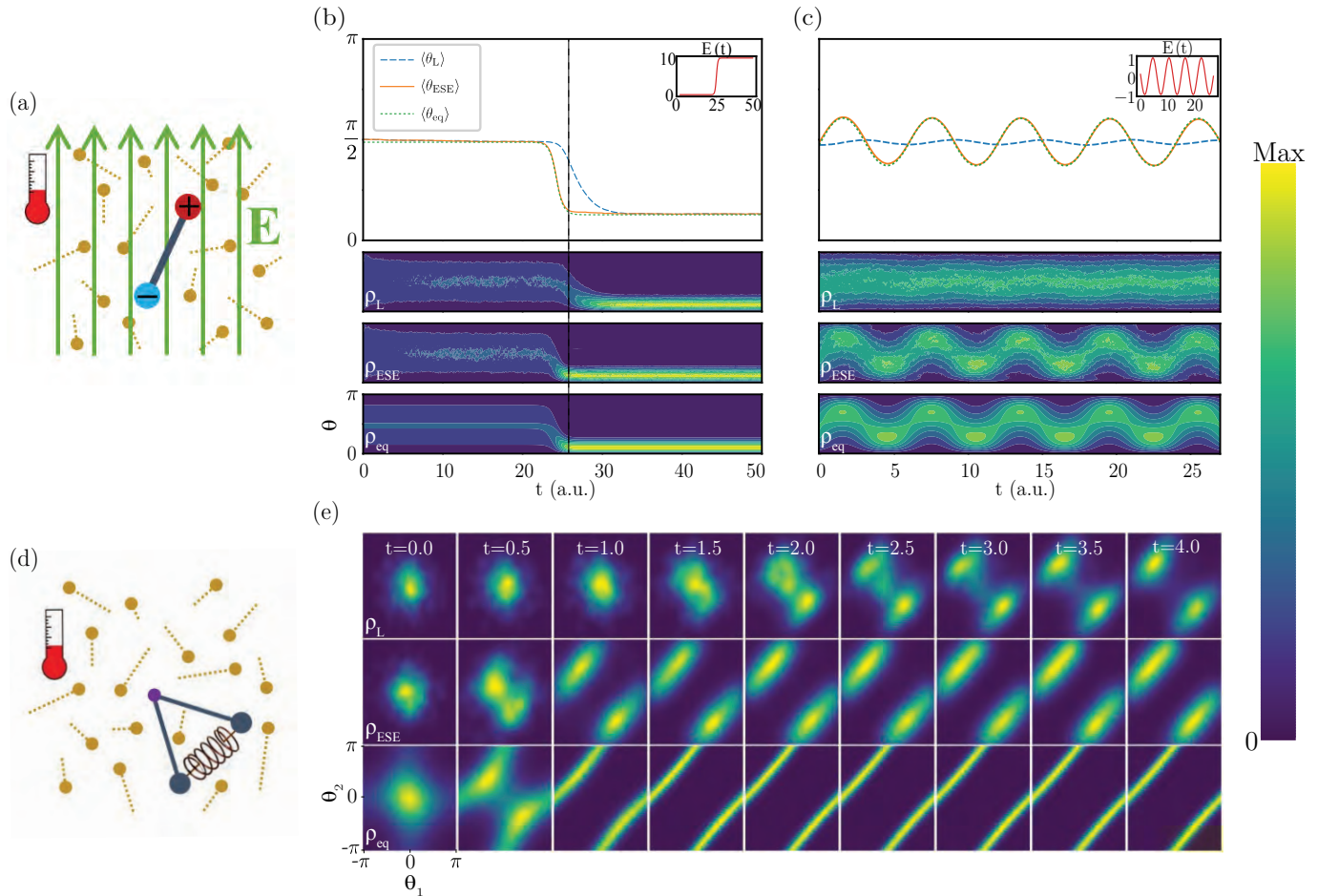


FIG. 1: Simulations demonstrate that ESE protocols produce densities closely tracking the equilibrium distribution in configuration space corresponding to the control parameters at each moment in time. **(a)** Schematic diagram of the ensemble considered in subplots **(b)** and **(c)**. An ensemble of electric dipoles are placed in a uniform, time-varying electric field. Due to these constraints, the the state of a dipole is specified by a polar coordinate  $\theta$  and an azimuthal angle  $\phi$  such that the system's configuration space is a (2D) sphere. **(b)** The electric field is varied sigmoidally in time, as shown in the inset. In the top panel, we show the average values of  $\theta$  over the entire ensemble for a system undergoing Langevin dynamics (dashed blue), ESE dynamics (solid orange), and for a Boltzmann distribution for the given electric field  $E(t)$ , denoted  $\rho_{eq}$  (dotted green). The three lower panels are the corresponding full distributions for  $\theta$  at all times. **(c)** Same as panel b for the sinusoidally varying electric field shown in the inset. **(d)** Schematic diagram of the ensemble considered in subplot **(e)**. An ensemble of two coupled pendula with time-varying coupling constant. The state of a coupled pendulum is specified by the two angular coordinates of the pendula,  $\theta_1, \theta_2 \in [-\pi, \pi)$ , such that the full system's configuration space is a torus. **(e)** The probability distributions of an ensemble of coupled pairs of pendula undergoing Langevin dynamics (top) and ESE dynamics (middle) plotted against the instantaneous Boltzmann distribution (bottom) for a coupling constant that changes from zero at small times to a negative value.

We now simulate the system for specified functions  $E(t)$ . The dynamics of this system are governed by a set of Langevin equations:

$$m(\ddot{\theta} - \sin \theta \cos \theta \dot{\phi}^2) = -\gamma \dot{\theta} - pE \cos \theta + \eta_\theta + F_{\text{ext},\theta}, \quad (17)$$

$$m(\sin \theta \ddot{\phi} + 2 \cos \theta \dot{\theta} \dot{\phi}) = -\gamma \sin \theta \dot{\phi} + \eta_\phi + F_{\text{ext},\phi}. \quad (18)$$

Note that, though we do not explicitly enforce the overdamped limit in Eqs. (17) and (18), we will effectively do so by means of parameter choices in our simulations. For

a specified  $E(t)$ , we numerically solve Eqs. (15) and (16) to find the ESE force (truncating above  $\ell = 5$ ) and then simulate the Langevin dynamics in both the presence and absence of this force for an “ensemble” of  $10^4$  dipoles. In units of  $\beta = m = p = 1$ , we simulate for  $\gamma = 20$ . Due to the noise terms in Eqs. (17) and (18), these are stochastic differential equations, which we simulate by means of a first-order Euler-Maruyama algorithm [19], with step sizes of  $dt = 0.01$  time units. Given the promotion of configuration space to a non-Euclidean manifold, the relation for the noise term is modified [20, 21]:

$\langle \eta_i(t) \eta_j(t') \rangle = (2\gamma/\beta) g^{ij} \delta(t-t')$ , where  $g^{ij}$  is the inverse metric of the manifold in question. For the (unit) sphere, the inverse metric is  $g^{\theta\theta} = 1$ ,  $g^{\phi\phi} = 1/\sin^2\theta$ , and all other entries are zero. Therefore, following the standard Euler-Maruyama treatment, we take  $\eta_\theta dt = \sqrt{2\gamma dt/\beta} \mathcal{N}(0,1)$  and  $\eta_\phi dt = \sqrt{2\gamma dt} \csc\theta/\beta \mathcal{N}(0,1)$ , where  $\mathcal{N}(0,1)$  is the Normal distribution with zero mean and unit variance. To deal with the spherical-polar coordinate singularities at  $\theta = 0$  and  $\theta = \pi$ , we temporarily rotate to a different local coordinate system where the poles are shifted away and numerically integrate a single time-step, whenever  $0 < \theta < \pi/10$  or  $9\pi/10 < \theta < \pi$ ; see Supplementary Material SM.2 for further details.

In Fig. 1 we plot both the mean value and the full probability distribution of  $\theta(t)$  for both the standard Langevin and ESE dynamics for two representative temporally varying electric fields, as described below. Due to the azimuthal symmetry of the problem, the azimuthal angle  $\phi$  is not affected by any temporal change in  $E(t)$ .

In Fig. 1(b), we consider a sigmoidally varying electric field,  $E(t) \sim E_0 + (\Delta E)S(t-t_c)$ , where

$$S(t) = (1 + e^{-t})^{-1} \quad (19)$$

is the logistic function,  $\Delta E = 10$  is the amplitude of the change of the electric field, and  $t_c$  is the transition time. For  $E_0$  small,  $\theta$  is primarily distributed about  $\pi/2$ , which corresponds to the equator. We note that for  $pE_0 \ll k_B T$ , the dipoles have no preferred direction, so they should be uniformly distributed throughout configuration space. However, the distribution appears non-uniform as a function of  $\theta$ . This is an artifact of our coordinate system: there is simply more phase space area at  $\theta = \pi/2$  (the equator) than elsewhere, such that the probability as a function of  $\theta$  should be non-uniform. For  $t \gg t_c$ , we find that, on average,  $\theta < \pi/2$ . This is physically sensible: the electric field is strong and directed in the  $\hat{z}$  direction such that the tendency of the dipoles will be to align with it. However, again as an artifact of our coordinate system, there is no probability density at  $\theta = 0$  as there is no phase space area at this pole. For  $t \sim t_c$ , in the absence of the ESE force, the system remains out of equilibrium for a finite period of time before eventually relaxing to the new equilibrium. However, when the ESE force is introduced, the system remains close to the equilibrium distribution at all times.

In Fig 1(c), we consider a sinusoidal electric field,  $E(t) \sim E \sin(t)$ . In this case, we see that the constantly changing field never allows the standard Langevin system to fully equilibrate; instead, the system oscillates with an approximate  $\pi/2$  phase-shift at a significantly smaller amplitude. The ESE dynamics, on the other hand, converge close to the equilibrium distribution at all points in time.

*Toroidal configuration space.*—Next, we consider toroidal configuration space, as exemplified by a system

of two pendula, each of mass  $m$  and unit length suspended vertically, and coupled to each other with a time-varying coupling constant  $\kappa(t)$ , as illustrated in Fig. 1(d). The potential may be modeled as

$$V(\theta_1, \theta_2, t) \simeq -(mg \cos \theta_1 + mg \cos \theta_2 - \kappa(t) \cos(\theta_1 - \theta_2)), \quad (20)$$

where  $\theta_1$  and  $\theta_2$  are angles of the respective pendula with respect to the  $z$ -axis. Given the periodicity in  $\theta_i$ , the configuration space of this system is the 2-torus,  $M = T^2 = [0, 2\pi] \times [0, 2\pi]$ . The Laplace operator for this manifold is

$$\Delta_{T^2} = \frac{\partial^2}{\partial \theta_1^2} + \frac{\partial^2}{\partial \theta_2^2}, \quad (21)$$

where one must recall the periodicity of the coordinates:  $\theta_i \sim \theta_i + 2\pi n$  for  $n \in \mathbb{Z}$ . We again employ a series expansion to solve Eq. (4). In this case, we carry out a 2D Fourier series. Considering that  $\Delta_{T^2} \exp i(m_1\theta_1 + m_2\theta_2) = -(m_1^2 + m_2^2) \exp i(m_1\theta_1 + m_2\theta_2)$ , we may write  $\rho_{\text{eq}} = \sum_{m_1, m_2} c_{m_1, m_2}(t) \exp i(m_1\theta_1 + m_2\theta_2)$  and easily deduce that

$$A = \gamma \sum_{m_1, m_2} \frac{\partial_t c_{m_1, m_2}(t)}{m_1^2 + m_2^2} e^{i(m_1\theta_1 + m_2\theta_2)}. \quad (22)$$

We again simulate this dynamical system for a given  $\kappa(t)$ . The governing Langevin equations are now

$$\begin{aligned} m\ddot{\theta}_{1/2} &= -\gamma\dot{\theta}_{1/2} - mg \sin \theta_{1/2} \\ &+ \kappa(t) \sin(\theta_{1/2} - \theta_{2/1}) + \eta_{\theta_{1/2}} + F_{\text{ext}, \theta_{1/2}}. \end{aligned} \quad (23)$$

As with the last example, the dynamics are not limited to the overdamped limit. For a specified  $\kappa(t)$ , we numerically solve the ESE force  $F_{\text{ext}}(t)$  by means of the Fourier series expansion (truncating above  $m_1 = m_2 = 10$ ) and then simulate the Langevin dynamics in both the presence and absence of this force. In units of  $\beta = m = g = 1$ , we simulate for  $\gamma = 20$ . We again employ an Euler-Maruyama algorithm with time step  $dt = 0.01$ . Due to the locally Euclidean metric of the torus, we need not deal with any geometric contributions to the noise terms and have  $\eta_{\theta_1} dt = \eta_{\theta_2} dt = \sqrt{2\gamma dt/\beta} \mathcal{N}(0,1)$ . For our simulations, we choose  $\kappa(t) \sim -\kappa_0 S(t)$ , where  $S(t)$  is defined by (19) so that the pendula are initially uncoupled but after some critical time  $t_c$  they are anti-coupled (we choose anti-coupling for clarity in the resulting figures). In Fig. 1(e), we display the resulting probability distribution for the coordinates  $(\theta_1, \theta_2)$  at several times near  $t_c$ . In the absence of the ESE force (top row), equilibration happens over a finite amount of time as the system relaxes to its new anti-coupled distribution. However, when the ESE force is added (second row), the resulting distribution agrees well with the calculated equilibrium

distribution  $\rho_{\text{eq}}(t)$  corresponding to the control parameter values at each moment in time (bottom row).

*Discussion.*—In previous studies, the notions of optimality and control often refer to specific protocols designed to minimize excess work or some other performance index when changing between two equilibria or non-equilibrium steady states in finite time [22–28]. The ESE framework we develop here may also be considered a control strategy, but ESE seeks only to minimize time to equilibration throughout the protocol without any constraints or penalties on the work required to do this. In principle, provided a smooth trajectory of control parameters, ESE should allow for arbitrarily rapid equilibrium switching of ensemble distributions. However, realizing the required forces in a laboratory setting would presumably preclude such a situation. Further, the theory itself breaks down in such a limit due to higher order effects ignored in a basic Langevin treatment, such as a finite characteristic timescale of the noise correlations. Therefore, for the range of timescales for which Eq. (2) applies, ESE yields a method to achieve controlled, swift equilibration. Furthermore, previous studies have analyzed the relation between the duration  $\tau$  of a protocol and the energy dissipated in carrying out a drive, concluding that for a variety of model systems, the energy dissipated is proportional to  $1/\tau$  [13, 29–31].

ESE protocols ensure a high degree of control throughout the drive. Not only do we enforce the mean, or the mean and variance (or any finite combination of moments) of the probability distribution, we place demands on the *entire* probability distribution at all times during the protocol. In fact, we can make an even stronger claim. Following [16], if a scalar field integrates to zero over a full manifold (without boundary), it may be written as the divergence of a vector field. Importantly, by integrating the LHS of Eq. (4) over any phase space manifold  $M$ , we see that

$$\int_M (-\gamma \partial_t \rho_{\text{eq}}) dV = -\gamma \frac{d}{dt} \int_M \rho_{\text{eq}} dV = -\gamma \frac{d}{dt} (1) = 0 \quad (24)$$

following conservation of probability. We conclude that for any arbitrary time-dependent potential described by some smooth set of coordinates, there will always be a corresponding ESE force that can enforce swift equilibration.

Finally, we note a further degree of freedom in the ESE condition defined by Eq. (7): The differential form  $d^\dagger P = \Delta A + d^\dagger C$  allows for an alternative, arbitrary choice of a harmonic one-form  $C$  if we make the replacement  $\gamma \partial_t \rho \rightarrow \gamma \partial_t \rho + d^\dagger C$  in Eq. (8). We also may include an arbitrary 2-form  $B$  by using Eq. (7), which leads to a class of inequivalent, though perhaps nonconservative, driving forces that can each enforce equilibration. These choices may allow for greater flexibility in solving Eq. (8) and finding appropriate forces for practical laboratory

applications.

*Conclusion.*—In this letter, we have successfully extended the ESE protocol to systems with nontrivial phase space topology. Our results could be useful for designing optimal strategies for manipulating a thermalized system of multiple canonical position variables swiftly through controlled parameter changes. Our methods can be used to calculate the necessary auxiliary forces to impose internal equilibrium dynamics in experimental settings. The derivation we present here is only valid for the overdamped limit. In future work, it will be interesting and useful to generalize our framework to include underdamped systems.

AGF is supported by the NSF GRFP under Grant No. DGE 1752814. SC is supported by NSF GRFP under Grant No. DGE 1106400 and the Berkeley Astrophysics Center Astronomy and Astrophysics Graduate Fellowship. MRD and DM were supported in part by the U. S. Army Research Laboratory and the U. S. Army Research Office under contracts W911NF-13-1-0390 (MRD and DM) and AWD-001219-G1 (MRD).

---

\* Electronic address: adamfrim@berkeley.edu

† Electronic address: deweese@berkeley.edu

- [1] A. Emmanouilidou, X.-G. Zhao, P. Ao, and Q. Niu, *Phys. Rev. Lett.* **85**, 1626 (2000), URL <https://link.aps.org/doi/10.1103/PhysRevLett.85.1626>.
- [2] M. V. Berry, *Journal of Physics A: Mathematical and Theoretical* **42**, 365303 (2009), URL <https://doi.org/10.1088%2F1751-8113%2F42%2F36%2F365303>.
- [3] E. Torrontegui, S. Ibáñez, S. Martínez-Garaot, M. Modugno, A. del Campo, D. Guéry-Odelin, A. Ruschhaupt, X. Chen, and J. G. Muga, in *Advances in Atomic, Molecular, and Optical Physics*, edited by E. Arimondo, P. R. Berman, and C. C. Lin (Academic Press, 2013), vol. 62, pp. 117 – 169, URL <http://www.sciencedirect.com/science/article/pii/B9780124080904000025>.
- [4] A. del Campo, *Phys. Rev. Lett.* **111**, 100502 (2013), URL <https://link.aps.org/doi/10.1103/PhysRevLett.111.100502>.
- [5] C. Jarzynski, *Phys. Rev. A* **88**, 040101 (2013), URL <https://link.aps.org/doi/10.1103/PhysRevA.88.040101>.
- [6] S. Deffner, C. Jarzynski, and A. del Campo, *Phys. Rev. X* **4**, 021013 (2014), URL <https://link.aps.org/doi/10.1103/PhysRevX.4.021013>.
- [7] A. Patra and C. Jarzynski, *New Journal of Physics* **19**, 125009 (2017), URL <https://doi.org/10.1088%2F1367-2630%2Faa924c>.
- [8] I. A. Martínez, A. Petrosyan, D. Guéry-Odelin, E. Trizac, and S. Ciliberto, *Nature Physics* **12**, 843 (2016), URL <https://doi.org/10.1038/nphys3758>.
- [9] S. An, D. Lv, A. del Campo, and K. Kim, *Nature Communications* **7**, 12999 (2016), URL <https://doi.org/10.1038/ncomms12999>.
- [10] M. Chupeau, B. Besga, D. Guéry-Odelin, E. Trizac, A. Petrosyan, and S. Ciliberto, *Phys. Rev. E* **98**,

- 010104 (2018), URL <https://link.aps.org/doi/10.1103/PhysRevE.98.010104>.
- [11] D. Guéry-Odelin, A. Ruschhaupt, A. Kiely, E. Torrontegui, S. Martínez-Garaot, and J. G. Muga, *Rev. Mod. Phys.* **91**, 045001 (2019), URL <https://link.aps.org/doi/10.1103/RevModPhys.91.045001>.
- [12] L. Kadanoff, *Statics, Dynamics and Renormalization* (World Scientific Publishing Company, 2000).
- [13] G. Li, H. T. Quan, and Z. C. Tu, *Phys. Rev. E* **96**, 012144 (2017), URL <https://link.aps.org/doi/10.1103/PhysRevE.96.012144>.
- [14] M. Chupeau, S. Ciliberto, D. Guéry-Odelin, and E. Trizac, *New Journal of Physics* **20**, 075003 (2018), URL <https://doi.org/10.1088%2F1367-2630%2Faac875>.
- [15] A. Baldassarri, A. Puglisi, and L. Sesta, *Phys. Rev. E* **102**, 030105 (2020), URL <https://link.aps.org/doi/10.1103/PhysRevE.102.030105>.
- [16] M. Nakahara, *Geometry, Topology and Physics* (CRC Press, 2003), 2nd ed.
- [17] J. D. Jackson, *Classical Electrodynamics, Third Edition* (Wiley, 1998), ISBN 9780471309321.
- [18] See Supplemental Material at [URL will be inserted by publisher] for details of a high temperature expansion, further simulation details, and a movie of a given simulation run as in Fig. 1(e).
- [19] P. E. Kloeden and E. Platen, *Numerical Solution of Stochastic Differential Equations* (Springer Berlin Heidelberg, 1992), URL <https://doi.org/10.1007/978-3-662-12616-5>.
- [20] N. Kumar and K. V. Kumar, *EPL (Europhysics Letters)* **86**, 17001 (2009), URL <https://doi.org/10.1209%2F0295-5075%2F86%2F17001>.
- [21] L. Apaza and M. Sandoval, *Phys. Rev. E* **96**, 022606 (2017), URL <https://link.aps.org/doi/10.1103/PhysRevE.96.022606>.
- [22] T. Schmiedl and U. Seifert, *Phys. Rev. Lett.* **98**, 108301 (2007), URL <https://link.aps.org/doi/10.1103/PhysRevLett.98.108301>.
- [23] T. Schmiedl and U. Seifert, *EPL (Europhysics Letters)* **81**, 20003 (2007), URL <https://doi.org/10.1209%2F0295-5075%2F81%2F20003>.
- [24] D. A. Sivak and G. E. Crooks, *Phys. Rev. Lett.* **108**, 190602 (2012), URL <https://link.aps.org/doi/10.1103/PhysRevLett.108.190602>.
- [25] P. R. Zulkowski, D. A. Sivak, G. E. Crooks, and M. R. DeWeese, *Physical Review E* **86**, 041148 (2012), ISSN 1539-3755, 1550-2376, URL <https://link.aps.org/doi/10.1103/PhysRevE.86.041148>.
- [26] P. R. Zulkowski, D. A. Sivak, and M. R. DeWeese, *PLoS ONE* **8**, e82754 (2013), ISSN 1932-6203, URL <https://dx.plos.org/10.1371/journal.pone.0082754>.
- [27] P. R. Zulkowski and M. R. DeWeese, *Physical Review E* **92**, 032117 (2015), ISSN 1539-3755, 1550-2376, URL <https://link.aps.org/doi/10.1103/PhysRevE.92.032117>.
- [28] C. A. Plata, D. Guéry-Odelin, E. Trizac, and A. Prados, *Phys. Rev. E* **99**, 012140 (2019), URL <https://link.aps.org/doi/10.1103/PhysRevE.99.012140>.
- [29] M. Esposito, R. Kawai, K. Lindenberg, and C. Van den Broeck, *EPL (Europhysics Letters)* **89**, 20003 (2010).
- [30] P. R. Zulkowski and M. R. DeWeese, *Phys. Rev. E* **89**, 052140 (2014), URL <https://link.aps.org/doi/10.1103/PhysRevE.89.052140>.
- [31] S. Campbell and S. Deffner, *Phys. Rev. Lett.* **118**, 100601 (2017), URL <https://link.aps.org/doi/10.1103/PhysRevLett.118.100601>.

# Supplementary Information for "Engineered Swift Equilibration for Arbitrary Geometries"

Adam G. Frim,<sup>1</sup> Adrienne Zhong,<sup>1</sup> Shi-Fan Chen,<sup>1</sup> Dibuyendu Mandal,<sup>1</sup> and Michael R. DeWeese<sup>1,2</sup>

<sup>1</sup>*Department of Physics, University of California, Berkeley, Berkeley, CA, 94720*

<sup>2</sup>*Redwood Center For Theoretical Neuroscience, University of California, Berkeley, Berkeley, CA, 94720*

(Dated: May 15, 2022)

## I. HIGH TEMPERATURE LIMIT OF DIPOLE MODEL

Suppose that we are in the high-temperature regime for the dipole model such that  $|pE(t)| \ll k_B T$ . In this case we can expand  $\exp \beta p E(t) \approx 1 + \beta p E(t) \cos \theta$  and the partition function as  $Z(t) = 4\pi + \mathcal{O}(\beta p E(t))^2$ . We then have, to the lowest order, the probability density as

$$\rho(\theta, \phi, t) = \frac{1}{4\pi} (1 + \beta p E(t) \cos \theta) \quad (1)$$

Taking the partial time derivative of the above gives us an equation of the form  $\Delta_{S^2} A = -(4\pi)^{-1} \gamma \beta p \dot{E} P_1(\cos \theta)$ , where  $P_1(x) = x$  is the first Legendre polynomial. Using the identity  $\Delta_{S^2} P_\ell(\cos \theta) = -\ell(\ell + 1) P_\ell(\cos \theta)$ , we immediately have the result

$$A = \frac{1}{8\pi} \gamma \beta p \dot{E} \cos \theta \quad (2)$$

Note that if the source term  $\gamma \partial_t \rho$  contained a constant a  $P_0(\cos \theta) = 1$ , Poisson's equation would be un-invertible; however, as the source term must integrate to zero, such terms are disallowed.

An interesting note: to first order the requisite force can be applied via a potential that can be practically produced just as a modulation in the original electric field. In particular we have

$$\vec{F} = \frac{dA}{\rho_{\text{eq}}} \approx -\frac{1}{2} \gamma \beta p \dot{E} \sin \theta \quad (3)$$

This is enforceable by modulating the applied electric field by  $\Delta E_{\text{ESE}}(t) = -\frac{1}{2} \gamma \beta \dot{E}_0$  where  $E_0$  distinguishes the electric field without the additional ESE contribution. If the original electric field were, for example, a sinusoid, this modulation would manifest as an out-of-phase contribution to the original field, resulting at first order in a small phase shift of the total signal.

## II. SIMULATION DETAILS

When numerically integrating (17) and (18) of the main text, the ODE becomes stiff and the numerics break down near the coordinate singularities at  $\theta = 0, \pi$ . Note that this is purely a feature of our local coordinate chart and not of the physics. Therefore, to simulate the system accurately, we must find ways of dealing with these poles. There are a number of schemes, though the conceptually simplest is simply to define a new coordinate chart and transform to this alternative whenever the system is close to a pole in the original coordinates. In this context, we define a primed set of coordinates  $(\theta', \phi')$  which are entirely analogous, i.e. a right-handed spherical coordinate system, though whose zenith is now oriented with the original  $x$ -axis (the coordinate singularity at  $\theta = 0$  now lies on the primed  $\hat{y}$ -axis). For completeness, we include the transformation in Table I.

Original Coordinates	Transformed Coordinates
$(x, y, z)$	$(z', x', y')$
$\theta$	$\arctan \left( \frac{\sqrt{\cos^2 \theta' + \sin^2 \theta' \sin^2 \phi'}}{\sin \theta' \cos \phi'} \right)$
$\arctan \left( \frac{\sqrt{\cos^2 \theta + \sin^2 \theta \cos^2 \phi}}{\sin \theta \sin \phi} \right)$	$\theta'$
$\hat{\theta}$	$\frac{\cos \theta' \sin \phi'}{\sqrt{\cos^2 \theta' + \sin^2 \theta' \cos^2 \theta'}} \hat{\theta}' + \frac{\cos \phi'}{\sqrt{\cos^2 \theta' + \sin^2 \theta' \cos^2 \theta'}} \hat{\phi}'$

TABLE I: Coordinate transformation used when  $0 < \theta < \pi/10$ ,  $9\pi/10 < \theta < \pi$  and is therefore close to coordinate singularities in spherical coordinates.